

ROTATION MEASURES OF LOW-LATITUDE EXTRAGALACTIC SOURCES AND THE MAGNETOIONIC STRUCTURE OF THE GALAXY

ANDREW W. CLEGG

Naval Research Laboratory, Code 4213, Washington, D.C. 20375

JAMES M. CORDES

Department of Astronomy, Cornell University, Ithaca, NY 14853

JOHN H. SIMONETTI

Department of Physics, Virginia Polytechnic Institute, Blacksburg, VA 24061

AND

SHRINIVAS R. KULKARNI

Division of Physics, Math, and Astronomy, California Institute of Technology, 105-24, Pasadena, CA 91125

Received 1991 June 3; accepted 1991 August 19

ABSTRACT

We have obtained Faraday rotation measurements of 56 extragalactic sources predominantly in the range $45^\circ < l < 93^\circ$, $|b| < 5^\circ$. The data complement the few rotation measures (RMs) that have been published for low-latitude extragalactic sources, and are used to probe the Galactic magnetic field and electron density to great distances. Within the longitude range sampled here, we find $RM(l) = 1600 \sin(l_0 - l) \text{ rad m}^{-2}$, with a null in RM occurring at $l_0 = 62^\circ$. Under the assumption of a uniform circular geometry for the magnetic field lines, the magnetoionic medium must exist to a Galactocentric radius $R_m \simeq 25 \text{ kpc}$ to produce the observed magnitudes of the RMs, where we have assumed that n_e and $|B|$ equal their local values of 0.03 cm^{-3} and $2.1 \mu\text{G}$ out to R_m . The medium must exist to an even greater radius if n_e and/or $|B|$ decrease with R , as is likely. The null in RM at l_0 confirms that a field reversal occurs interior to R_0 (the radius of the solar orbit about the Galactic center) and requires that the product quantity $n_e|B|$ be greater inside the field-reversed region than in the local ISM. Comparison of extragalactic and pulsar RMs along nearly coincident lines of sight is consistent with at least one field reversal exterior to R_0 . An anomalous RM contribution of $\gtrsim 1000 \text{ rad m}^{-2}$ is found at $l = 92^\circ$, $b = 0^\circ$, with an angular size of $\sim 1^\circ\text{--}8^\circ$. The phenomenon is akin to enhanced RMs observed behind the Cygnus region. The majority of our sources are components of double-lobed objects with lobe separations of $30''\text{--}200''$. This allows us to study variations in Galactic Faraday rotation over small angular scales. The differences exceed those expected from a large-scale ordered field by more than two orders of magnitude. The implied linear scales for fluctuations in the magnetoionic medium are $\sim 0.1\text{--}10 \text{ pc}$. We are able to explain the small-scale variations in RM solely in terms of previously observed electron density turbulence in the interstellar medium.

Subject headings: Galaxy: general — ISM: magnetic fields — polarization — radio continuum: galaxies

1. INTRODUCTION

At radio wavelengths, the diffuse magnetoionic component of the ISM is best probed by Faraday rotation measurements. For a linearly polarized wave traversing the medium, the observed polarization position angle at a wavelength λ is $\phi(\lambda) = \phi_0 + RM\lambda^2$, where ϕ_0 is the unrotated position angle and the *rotation measure* (RM) is the line-of-sight integral

$$RM(\text{rad m}^{-2}) = \frac{e^3}{2\pi m_e^2 c^4} \int n_e \mathbf{B} \cdot d\mathbf{l}; \quad (1)$$

here e , m_e , and c are, respectively, the electron charge and mass, and the speed of light. Numerically, $e^3/(2\pi m_e^2 c^4) = 810$ for the electron density n_e in cm^{-3} , the magnetic field B in μG , and the path length l in kpc. The contribution to RM is positive for a magnetic field pointed toward the observer.

To date most Galactic Faraday rotation measurements have been obtained toward pulsars (e.g., Lyne & Smith 1989) or extragalactic sources (e.g., Simard-Normandin, Kronberg, & Button 1981). The pulsar data probe the Galactic plane component of the medium. Since pulsar distances can often be independently derived, the data also provide information on

the variation of RM along the line of sight. Also, dispersion measurements toward the pulsar give the column density (or *dispersion measure*, DM) along the line of sight so that the electron density-weighted longitudinal field strength can be separately determined. Few pulsars are known beyond a Galactocentric radius of $\sim 15 \text{ kpc}$, so what we know about the magnetoionic medium through pulsars is generally limited to less than this distance. Extragalactic sources can potentially provide information about the Galactic medium to great distances, since the line of sight toward these objects extends through the entire Galaxy. However, the Galactic plane component of the magnetoionic medium has not been effectively probed with extragalactic RMs because the existing data are almost exclusively for sources at latitudes greater than 10° , where the line of sight passes out of the medium after a distance projected on the plane of $\lesssim 5 \text{ kpc}$, assuming a scale height for the medium of 1 kpc .

In this paper, we report the results of a Faraday rotation survey of 56 extragalactic sources over the longitude range $45^\circ < l < 93^\circ$. This work complements the existing body of rotation measure data in several important ways. First, the sources are concentrated at low Galactic latitudes, with 82% of

the objects within 5° of the plane. With a scale height for the magnetoionic ISM of 1 kpc, our low-latitude data probe the medium to distances ≥ 12 kpc projected on the plane. Second, the density upon the sky of low-latitude sources (~ 360 sources sr^{-1}) is two orders of magnitude greater than for previous surveys. Such a dense sample is excellent for assessing models of the Galactic magnetic field since the models generally predict complicated variations of RM with longitude. Third, when combined with pulsar rotation measures our data enable us to study field reversals both interior and exterior to the solar circle. Fourth, the majority of the objects are components of double-lobed radio sources with lobe separations of $30''$ – $200''$. This allows us to study variations in Galactic Faraday rotation over small angular scales.

In § 2 we present a brief summary of what is known to date about the Galactic magnetic field. Several models for the field based on previous RM surveys are reviewed. We concentrate on their predictions for RMs in the region of the sky sampled here. In § 3, the observing and data reduction strategies are discussed, and we give an example of the process of determining RM from the raw position angle data. In § 4 we discuss the method of locating and removing sources from our original sample which we believe are affected by intrinsic polarization effects. If attributed to Galactic Faraday rotation these effects would produce incorrect results. In § 5 we provide a general discussion of the observed RMs. The data are discussed in more detail beginning with § 6. There we derive the extent of the magnetoionic medium and the position of a field reversal interior to the solar circle. We also discuss the effect of the North Polar Spur on the data and present a comparison of the extragalactic data with pulsar RMs along similar lines of sight. In § 7 we derive the physical properties of a remarkable region of anomalous RM observed in the plane at 92° longitude. In § 8 we discuss variations in RM over small angular scales and what the results suggest with respect to electron density turbulence in the ISM. The conclusions are listed in § 9 where we have also incorporated a schematic summary of our results.

2. PREVIOUS MODELS OF THE GALACTIC MAGNETIC FIELD

What we know to date about the Galactic field has been summarized in Heiles (1987) and Kulkarni & Heiles (1988) and references therein. The theory of the field formation is reviewed by Zweibel (1987). In this section we briefly review several models of the Galactic magnetic field, emphasizing their predictions for the region of sky observed in this survey. (Reference to Fig. 12 of § 9 will clarify the geometry of the field configuration as discussed below).

Manchester (1974) used 28 pulsar RMs to analyze the “local” field to 1 kpc distance, and found a field magnitude and direction $2.2 \pm 0.4 \mu\text{G}$ toward $l = 94^\circ \pm 11^\circ$. Thomson & Nelson (1980, hereafter TN) used 48 pulsars with distances out to 3 kpc to analyze the field. There was some overlap with the data used by Manchester. They found a field of $3.5 \pm 0.3 \mu\text{G}$ amplitude pointing toward $l = 74^\circ \pm 10^\circ$. Manchester and TN assumed the field geometry was “longitudinal” (i.e., no curvature to the field lines over the limited distance they are probed). Manchester discounted sources believed to be influenced by the North Polar Spur (NPS) which is a region of magnetic anomaly extending northward from the plane roughly at $l = 30^\circ$. The NPS produces a positive contribution to RMs in this region.

Simard-Normandin & Kronberg (1980, hereafter SK) used a large number of extragalactic RMs (543 in all) to test com-

prehensive models of the large-scale Galactic field. They identified several regions where RMs differ systematically from an ordered field. Of particular interest for the present analysis is their region C ($0^\circ \lesssim l \lesssim 60^\circ$, $b > 0^\circ$) where RMs are *positive*, opposite to that expected from the general trend of RMs with longitude. The NPS is probably partially responsible for region C. SK fit circular and spiral magnetic field models to the data and find that many of the features in their RM sky (including region C) can be reproduced by either model when magnetic field reversals are invoked. Both models have constant magnetic field amplitude of $\sim 1 \mu\text{G}$ over Galactic radii of 4 to ~ 15 kpc. The best circular model has one field reversal approximately 2 kpc interior to the solar circle (taken to be $R_0 = 10$ kpc¹). The bisymmetric spiral model has two reversals inside R_0 , the nearest at ~ 2 kpc distance, with a spiral pitch angle of $\sim 14^\circ$ (i.e., the local field points toward $l \simeq 76^\circ$). Neither model invokes field reversals *outside* of the solar circle.

Inoue & Tabara (1981, hereafter IT) use 637 extragalactic RMs (from Tabara & Inoue 1980), 39 pulsar RMs, and optical polarization of 5070 stars to study the Galactic field. Out of the sample of extragalactic RMs, however, IT argue that the northern hemisphere data are corrupted by the presence of the NPS and other magnetoionic anomalies, and discount sources in the southern hemisphere within 30° of the plane because of difficulties resolving $n\pi$ ambiguities in the position angle data. They effectively sampled about 25% of the sky and are not sensitive to the distant Galactic plane component. With their derived z -scale height of 580 pc their data at $b < -30^\circ$ samples the field only out to a distance projected on the Galactic plane of about 1 kpc. From comparison of pulsar RMs and DMs ($\text{DM} = \int n_e dl$), they derive a mean magnetic field amplitude of $1.6 \pm 0.4 \mu\text{G}$. Using all data (extragalactic, pulsar, and optical) they find a field direction toward $l = 100^\circ \pm 10^\circ$.

Sofue & Fujimoto (1983, hereafter SF) used the Tabara & Inoue (1980) data without the constraint in b to fit a bisymmetric spiral field with the field lines roughly coincident with spiral arms as traced by H II regions. The magnetic field amplitude and mean interstellar electron density are assumed to have z scale heights of approximately 1 kpc, and scaling in Galactocentric distance R of $\propto 1/R$, normalized to local values ($R = R_0$) of $3 \mu\text{G}$ and 0.03 cm^{-3} . The field strength is 0 for $R < 4$ kpc and $R > 15$ kpc, and its direction reverses from one spiral arm to the next. The local tangent to the field is toward $l = 85^\circ$.

Rand & Kulkarni (1989) used 163 pulsar RMs of Hamilton & Lyne (1987) to model the field. They exclude pulsars toward which the mean magnetic field amplitude is greater than $2 \mu\text{G}$ in the range $0^\circ \lesssim l \lesssim 60^\circ$, under the assumption that the data are corrupted by the NPS and do not represent RMs due to a large-scale field. Their best fit is a concentric ring model with a local magnetic field amplitude of $1.3 \pm 0.2 \mu\text{G}$. They assume the amplitude varies sinusoidally with R , which avoids requiring abrupt reversals in B . They find that the maximum amplitude is $2.15 \mu\text{G}$, with a local amplitude ($R = R_0$) of $1.6 \mu\text{G}$. The nearest reversal interior to the solar circle is at a distance of 650 ± 90 pc measured toward the Galactic center. An additional interior reversal occurs at a distance of ~ 6250 pc ($R = 3.75$ kpc), and one *exterior* reversal at a distance of about 2450 pc ($R = 12.45$ kpc).

¹ To conform with previous analyses of Galactic RMs, throughout this paper we take the distance to the Galactic center, R_0 , to be 10 kpc. Current IAU convention is $R_0 = 8.5$ kpc.

Among these models there is little consensus on the strength, direction, and geometry of a large-scale Galactic field. Naively averaging the magnetic field amplitudes from the models gives a value $2.1 \pm 1.0 \mu\text{G}$. The average direction is toward $l = 87^\circ.5 \pm 10^\circ.9$ with half of the estimates being greater than 90° and half less than 90° . The component of the magnetic field direction perpendicular to the plane is not well constrained by the models and is not of immediate importance to the present work which probes the field within the Galactic plane. Of those models specifying more than the local field, two indicate a concentric ring geometry and two indicate a bisymmetric spiral field. However, almost all models (five out of six) require at least one field reversal (most being interior to the solar circle) and all models for which a random component is invoked require that the random field amplitude be at least a sizable fraction of the mean field.

While some of the models have been based on large samples of RMs all of them are derived with, or checked against, a sparse sample of low-latitude data (typically $\ll 10$ sources sr^{-1}). It is our opinion that the model generally produce poor fits to low-latitude extragalactic RMs. The data presented here—360 sources sr^{-1} at low latitudes—provide the best constraint to date of the Galactic magnetic field on large scales and clearly demonstrate the shortcomings of the Galactic field models.

3. OBSERVING AND DATA REDUCTION

Potential sources were obtained from a 327 MHz Westerbork survey and other data provided by M. Stevens & C. Heiles (1986, private communication) and S. R. Kulkarni (1986, private communication). Additional sources were identified from the 1400 MHz survey of Garwood, Dickey, & Perley (1986). A pilot observing program was carried out in 1986 July using the Very Large Array.² We obtained brief (< 5 minute) integrations of each source at $\lambda = 20$ cm to ascertain their suitability for further study in terms of brightness (both total and polarized flux density) and source structure. Out of the 44 suitable objects found, 17 possessed single emission components which were suitable for measuring RM, while 22 of the sources were classic double-lobed objects. The remaining five sources possessed three polarized components suitable for RM measurements. Our initial data sample was therefore composed of 76 source components. Data selection criteria, discussed below, reduced the number of components used in the final analysis. Flux densities for the remaining objects ranged between 0.02 and 6 Jy beam^{-1} (0.3 Jy beam^{-1} typical); percentage polarizations ranged from 0.5% to 25% (5% typical). The naming convention for the individual components of multicomponent sources is our own. The components are labeled "A," "B," or "C," in descending order of declination.

In 1986 August the sources were reobserved with the B-configuration array, at which time longer integrations were obtained and several standard sources were observed to provide accurate amplitude, phase, and polarization calibration. The synthesized beamwidth (FWHM) was $\sim 4''.2$. Subsequent (u, v) -data editing and weighting increased the beam size (see below). Six L-band frequencies were used: 1385.1, 1415.1, 1464.9, 1514.9, 1634.9, and 1664.9 MHz. The frequencies were chosen to cover as large a range in λ^2 as possible

while avoiding well-known interference signals both internal and external to the array. Continuum bandwidths of 12.5 MHz were used at each frequency to minimize depolarization. We employed two separate IF systems for simultaneous acquisition of data at two frequencies. Three sequential sets of observations were made on each source, yielding the desired six frequencies. Integration times varied, ranging from 6 to 10 minutes for each frequency pair. Complex (u, v) -visibilities from cross-correlations between circular polarizations of all antennas were used to produce images of the Stokes parameters I , Q , and U for each field.

The primary flux density and position angle calibrator was 3C 286 (1328 + 30), which was assumed to have a flux density of 13.6 Jy beam^{-1} and no Faraday rotation. Its observed rotation measure is $-1 \pm 0.2 \text{ rad m}^{-2}$ (Simard-Normandin et al. 1981), so systematic errors introduced in our data by assuming RM = 0 are small. Ionospheric contributions to RM are $\lesssim 1\text{--}10 \text{ rad m}^{-2}$; interplanetary contributions are less (Thompson, Moran, & Swenson 1986). The polarization calibrator 2352 + 495 was observed at 2 hr intervals. The data were used to correct for the elliptical response of the nominally circularly polarized feeds. Fifteen additional sources were observed at least once during the observing period as secondary amplitude and phase calibrators.

The (u, v) -data were processed using NRAO's Astronomical Image Processing System. A uniform weighting function was applied (deemphasizing short baselines), and the data were tapered over baseline length ($1/e$ level at 30 k λ) to reduce "ringing" sidelobe structure due to finite (u, v) -plane coverage. Weighting and tapering the data increased the synthesized beamwidth to approximately $6''$ (FWHM). The data were Fourier transformed and subsequently CLEANed (Clark 1980) to deconvolve the beam response from the image. We produced images of the three Stokes parameters at each of the six frequencies for all fields. From these images, maps of the polarized flux density F_p and polarization position angle ϕ were also created, where

$$F_p = (U^2 + Q^2)^{1/2}, \quad (2)$$

$$\phi = \frac{1}{2} \tan^{-1}(U/Q). \quad (3)$$

A map pixel was not used in the analysis if its Q or U flux density did not exceed 0.5 mJy. Occasionally, data for a particular frequency were unusable due to interference, so that fewer than six position angle measurements were obtained. A total of 1320 maps were created representing 44 fields. Total intensity contour plots of each field are presented in Appendix C of Clegg (1991). Measured rms flux density variations were 0.7 mJy in a sample of five total intensity images. The result is twice the theoretical noise limit (0.35 mJy) computed from quoted system parameters (Napier & Crane 1982), with the difference at least partly due to the limited (u, v) -plane coverage we obtained during the short integrations.

In theory, position angle errors in the limit of large $F_p/\sigma_{Q,U}$ are $\sigma_\phi = 0.5\sigma_{Q,U}/F_p$, where $\sigma_{Q,U}$ is the rms variation in the Q or U images. In practice, we find the reliable estimation of σ_ϕ quite difficult. The measured 1464.9 MHz flux densities for 29 sources were a constant factor of ~ 5 lower than at the other frequencies. The cause of the discrepancy is not clear, but it has been noted by other VLA observers. For the affected sources, flux densities measured at the other five frequencies were either consistent with one another to within uncertainties or could be fitted within uncertainties by a simple power law in frequency.

² The VLA is part of the National Radio Astronomy Observatory, which is operated by Associated Universities, Inc., under contract to the National Science Foundation.

The 1464.9 MHz flux densities were clearly anomalous. The polarization percentage and position angle at 1464.9 MHz were apparently unaffected. We conclude that the flux density “drop outs” are instrumental in origin and are not intrinsic to the sources, and that they do not otherwise effect our polarization measurements. Their presence, however, introduces uncertainties into the determination of σ_ϕ . We resorted to an empirical method for estimating σ_ϕ , where the variation in position angle $\tilde{\sigma}_\phi$ was measured across a set of extended sources which contained no apparent intrinsic gradient in position angle. For each of these sources, the measured $\tilde{\sigma}_\phi$ yielded an effective $\tilde{\sigma}_{Q,U}$ through $\tilde{\sigma}_{Q,U} = 2F_p \tilde{\sigma}_\phi$, where F_p is the polarized flux density of the source. The average value of $\tilde{\sigma}_\phi$ determined from the set of extended sources was subsequently used to bootstrap position angle uncertainties for the remaining sources. For a source of polarized flux density F_p , we estimated $\sigma_\phi \approx 0.5\tilde{\sigma}_{Q,U}/F_p$. A shortcoming to this empirical method is that we do not know what fraction of the position angle uncertainties for the set of extended sources may be due to intrinsic gradients in RM or RM variations imparted from small scale structure in the Galactic distribution of $n_e B$. However, we note that the values of χ^2 (see below) for the RM fits compare favorably with the expected distribution.

The process of determining rotation measures is illustrated in Figures 1 and 2. In Figure 1 contour plots of the continuum emission from sources 1914+149 A (north) and B (south) are shown at each frequency. Overlaid on the plot are polarization position angle vectors, the lengths of which are proportional to the polarized flux density. The position angle is measured eastward (counterclockwise) from north (top). To obtain an esti-

mate of the position angle at each frequency, the direction of the vectors is averaged over approximately one synthesized beam. The resultant position angles for source A are plotted in Figure 2. Position angles are computed modulo π , and a linear fit to $\phi(\lambda^2)$ may “wrap” beyond the $\pm\pi/2$ rad limit. Consequently, data points are shifted in integer units of π to recover the correct rotation measure. Shifts of magnitude $\leq 2\pi$ are applied to each position angle measurement, and a linear regression to the resultant ϕ versus λ^2 data are computed. For a set of six position angles, $5^5 = 3125$ such fits are tried. The quality of each regression is quantified by computing χ^2 ,

$$\chi^2 = \frac{1}{N-2} \sum_{i=1}^N \frac{(\phi_i - \phi_{i,0})^2}{\sigma_i^2}, \quad (4)$$

where N is the number of data points, and ϕ_i , $\phi_{i,0}$, and σ_i are, respectively, the measured position angle, the fit to the position angle, and the position angle uncertainty at frequency i . A good fit is one for which $\chi^2 \sim 1$, although a distribution of values is expected (Bevington 1969). Values of $\chi^2 \ll$ or $\gg 1$ are unlikely to occur. The solid line in Figure 2 is a least-squares fit to the shifted data points for 1914+149A which yielded the minimum value of χ^2 ; its slope is the adopted rotation measure for that source. For comparison, the second-best fit to the data is shown (hollow circles fitted by the dashed line). In this particular instance, there is a clear distinction in the quality of the two fits. In most cases, the accepted rotation measure was the slope of the minimum χ^2 fit, where the minimum was well-defined and significantly less than the next best fit. Two or more acceptable fits were found for 1919+162A, 1945+24A,

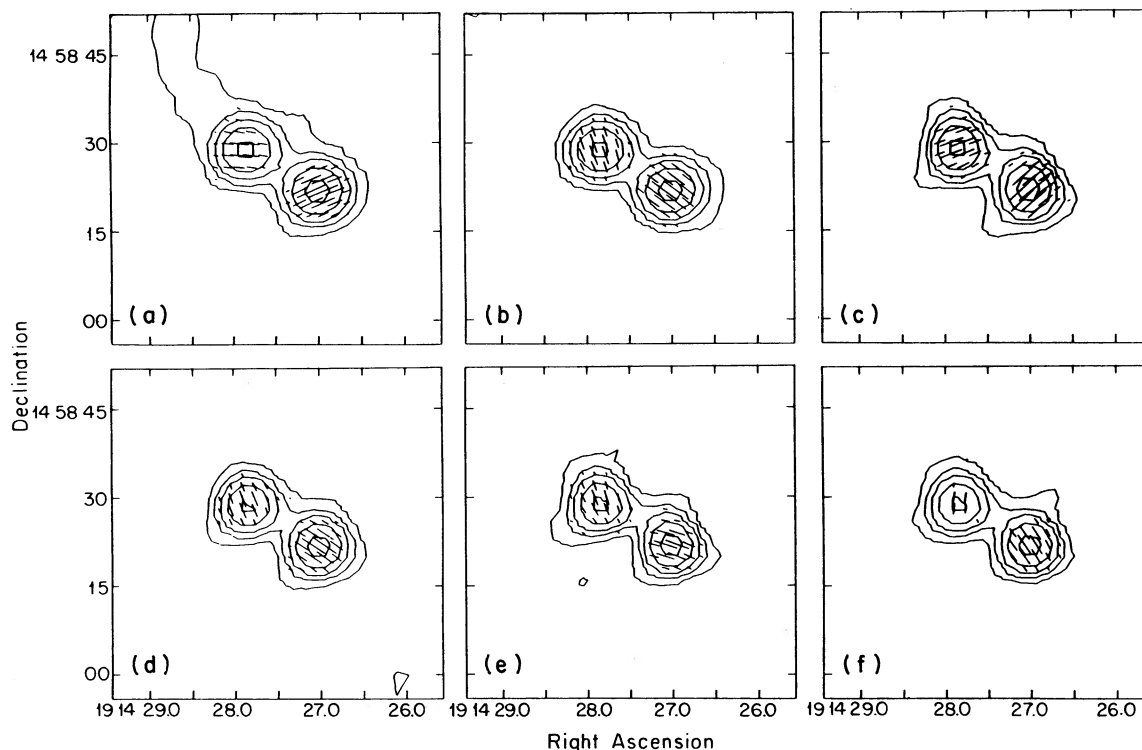


FIG. 1.—Example of polarization data for the 1914+149 region. Source A is the northern component, source B the southern. Polarization vectors are overlaid on total flux density contours at six frequencies: 1385.1, 1415.1, 1464.9, 1514.9, 1634.9, and 1664.9 MHz (panels a–f, respectively). Lengths of the vectors are proportional to polarized flux density, and their direction measured $\pm\pi/2$ eastward (counterclockwise) from north (top) is the position angle modulo π . Position angles are averaged over one synthesized beamwidth about the pixel of maximum polarized flux density to obtain a position angle estimate at one frequency for a given source.

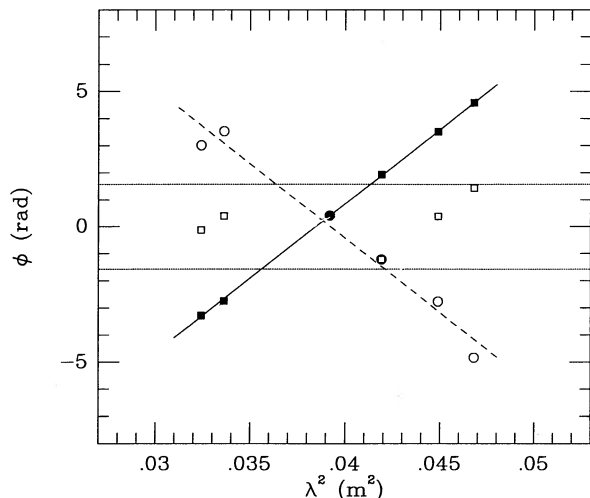


FIG. 2.—Example of rotation measure fit for source 1914+149A. Polarization position angles are originally determined modulo π between $\pm\pi/2$ (hollow squares between dotted lines), and are shifted in units of π up to a maximum of $\pm 2\pi$ until a minimum χ^2 fit is obtained (filled squares fitted by solid line). For comparison, the second-best fit is also plotted (hollow circles fitted by dashed line). Estimated error for each position angle determination is ≈ 0.1 rad (1 σ) and is smaller than the data points themselves.

1953+28B, 2029+20A, and 2052+46B. For these sources, we adopted the value of RM that was consistent with nearby sources.

4. RELIABILITY OF MEASURED RM

We attempted to remove sources whose polarization characteristics are corrupted by intrinsic effects. The major causes are discussed by Gardner & Whiteoak (1966), Kronberg, Conway, & Gilbert (1972), and Vallée (1980). They include the possibility of observing through a range in wavelength where the synchrotron optical depth $\tau \approx 1$, and the polarization direction makes a transition from parallel ($\tau > 1$) to perpendicular ($\tau < 1$) to the projected magnetic field direction. Additionally, multiple unresolved emission components with differing spectral indices and polarization characteristics can produce complicated wavelength dependent variations in ϕ , as can sources with significant gradients in Faraday rotation across or through the emission region. Our test for the presence of these effects is the *linearity* of $\phi(\lambda^2)$ as judged by χ^2 (eq. [4]) since optical depth or multiple component effects will produce oscillatory or otherwise nonlinear behavior in $\phi(\lambda^2)$. We compared the distribution of χ^2 values with the predicted distribution (Bevington 1969). The distribution of χ^2 values from our data is presented in Figure 3. For convenience, five sources with $\chi^2 \geq 10$ were not plotted. The histogram is only for sources for which we had six valid position angles to facilitate a comparison with the theoretical distribution of χ^2 which depends on the number of fitted points. This distribution, shown by the solid line, is normalized to the total number of sources within the 99% confidence level ($\chi^2 = 3.3$), since less than one source should have χ^2 outside this level. Larger χ^2 values are assumed to be due to intrinsic polarization effects rather than statistical fluctuations. After rejecting all sources outside the 99% confidence level in χ^2 , 56 of the original sample of 76 RMs remained.

5. RESULTS

Position angle data for each source are plotted in Figure 4. Table 1 gives the name, coordinates (Galactic and equatorial), flux density, percentage polarization, rotation measure with error, and χ^2 for each source. The coordinates are given for the map pixel of peak total flux density, where the size of each pixel = $2'' = 0.13$ s = $0^{\circ}0006 = 0.33$ beamwidth (FWHM). Sources chosen for further analysis based on the quality of the fit are footnoted in Table 1. The remaining sources were discounted by our selection criteria (§ 4) but are included in the table and in Figure 4 for completeness. Rotation measures as functions of Galactic longitude and latitude are presented in Figures 5 and 6, respectively. Figure 7 shows RM as a function of longitude when the data are averaged over bins of width 5° , excluding those sources surrounded by dashed lines in Figure 5 (those data are either anomalous or are from a different survey, and are discussed later).

The data show a strong correlation between RM and l caused by the large-scale field. Over the observed range the data are well fitted by the function

$$\text{RM}(l) = \text{RM}_0 \sin(l_0 - l) \approx \text{RM}_0(l_0 - l), \quad (5)$$

with all angles in radians, $\text{RM}_0 = 1607$ rad m^{-2} , and $l_0 = 1.085$ rad = $62^{\circ}.1$ is the Galactic longitude at which a null in the extragalactic RMs is observed. The function is shown in Figure 5. The rms deviation about the fit is 157 rad $\text{m}^{-2} \approx 0.1$ RM_0 . Both emission regions of a source at $b < 0^{\circ}.01$ have enhanced RMs. Presumably this is due to the line of sight remaining below one scale height of the magnetoionic medium for a large distance, as this source is the lowest latitude source observed in the survey. Alternatively a discrete disturbance lies along the line of sight. There are no other nearby sources exhibiting enhanced RMs, so it is difficult to determine the origin of the enhancement. These data have not been used in the fit or in the computation of the rms deviation about the fit; they are surrounded by dashed lines in Figure 5. The intriguing cluster of sources with anomalous positive RMs at $l = 92^{\circ}$ was

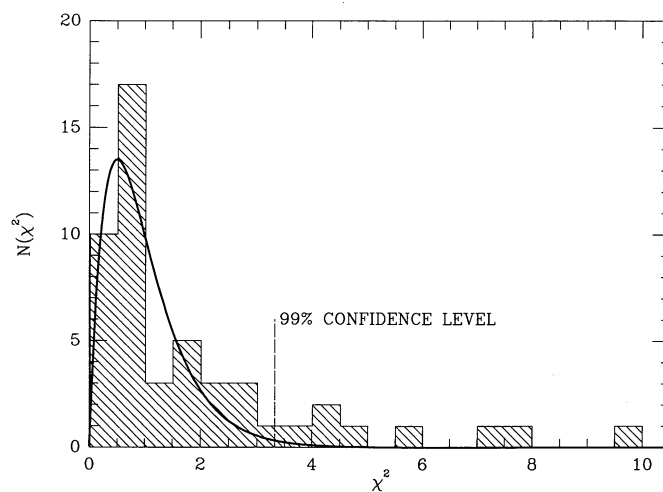


FIG. 3.—Distribution of χ^2 values (eq. [4]) from the data. Sources with $\chi^2 > 10$ are not shown, nor are sources for which valid position angle measurements were obtained at fewer than six frequencies. The curve is the expected distribution normalized to the total number of sources for which χ^2 fell below the 99% confidence level (dashed line). Fewer than one source should have exceeded this level. Those that did were assumed to possess intrinsic polarization effects and were not used in the analysis of the Galactic field.

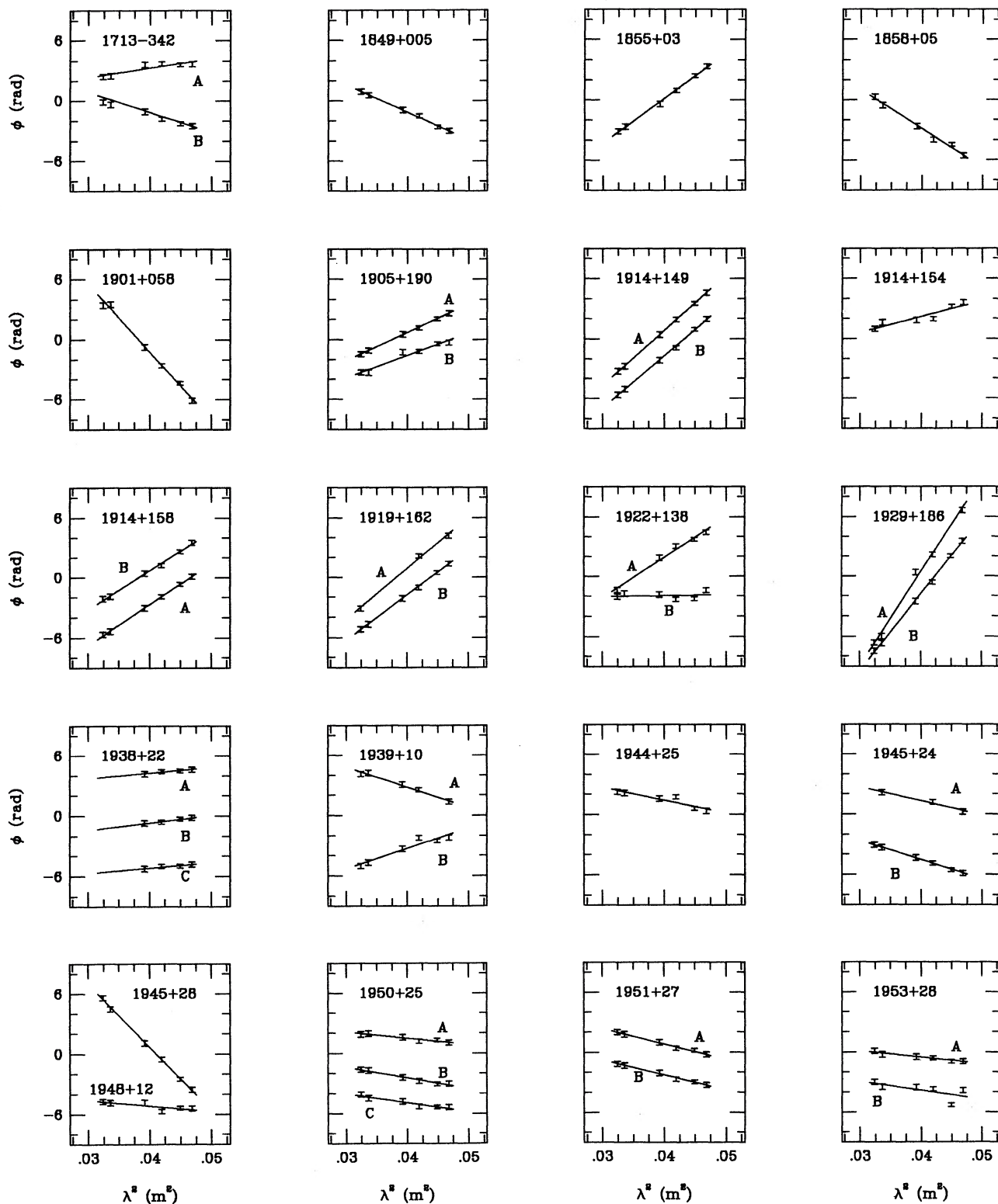


FIG. 4.—Minimum χ^2 fit to $\phi(\lambda^2)$ for all sources. Error bars are $\pm 3\sigma$. Slope of the linear fits is RM.

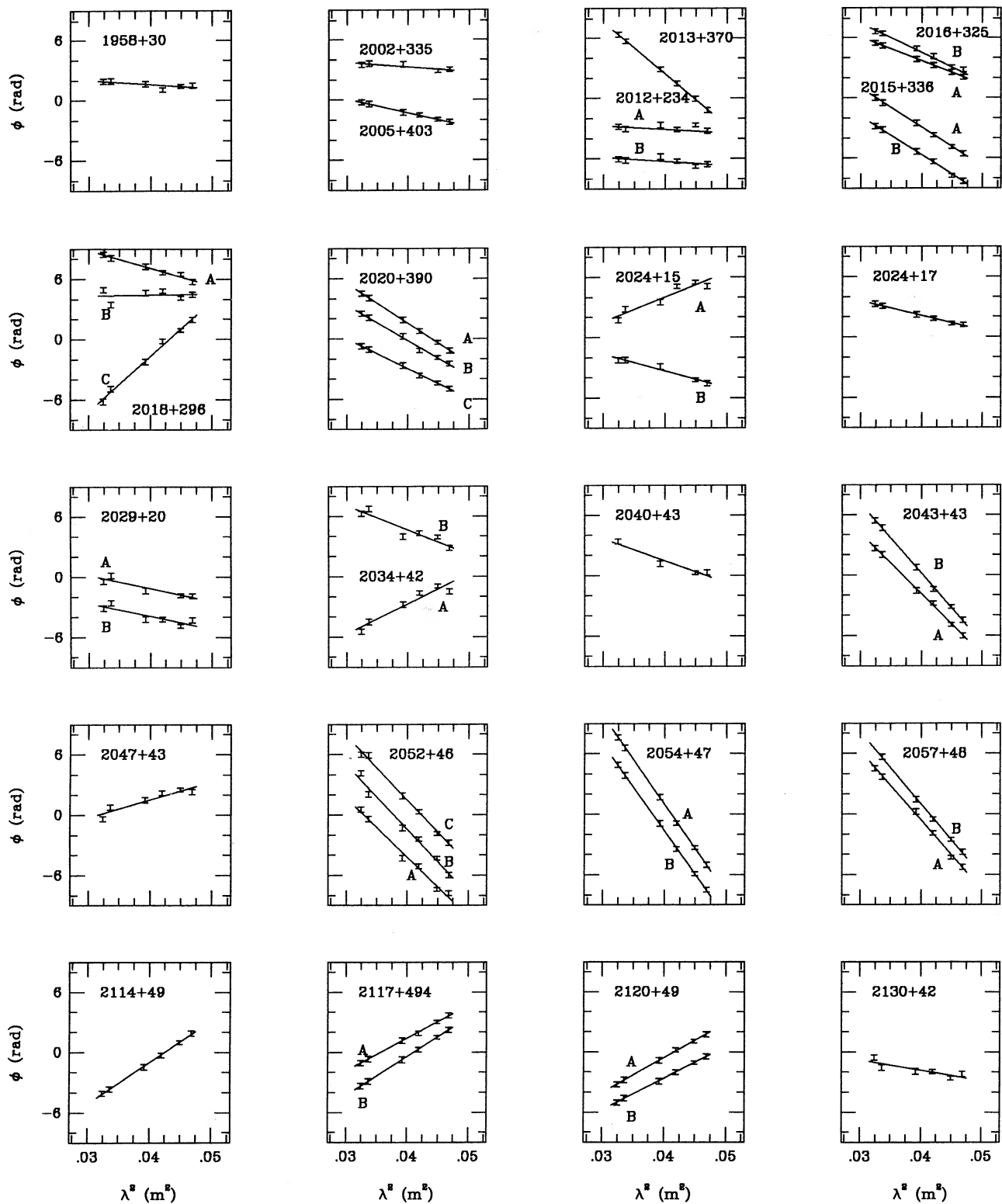


FIG. 4—Continued

TABLE 1
BEST FIT ROTATION MEASURES

Source	l (deg)	b (deg)	α (1950)	δ (1950)	F (Jy)	P (%)	RM (rad m ⁻²)	χ^2
1713-342A	352.0672	2.2484	17 13 05.3	-34 14 58	0.157	8.1	96 +/- 7	10.8
1713-342B ^a	352.0662	2.2498	17 13 04.8	-34 14 58	0.210	5.8	-169 +/- 9	1.1
1849+005	33.5068	0.1942	18 49 13.6	00 31 53	0.778	2.6	-275 +/- 4	4.0
1855+03	36.5593	0.0019	18 55 32.2	03 09 11	0.892	5.8	448 +/- 4	7.3
1858+05	38.6002	0.2270	18 58 30.7	05 04 05	0.104	7.8	-391 +/- 7	11.0
1901+058	39.5726	-0.0398	19 01 16.1	05 48 26	0.527	2.4	-679 +/- 11	7.0
1905+190A ^a	52.5058	5.5904	19 05 11.6	19 51 48	0.056	4.4	281 +/- 9	0.1
1905+190B ^a	52.5014	5.5904	19 05 11.1	19 51 34	0.830	0.3	226 +/- 12	4.1
1914+149A ^a	49.1940	1.3646	19 14 27.9	14 58 30	0.182	3.0	550 +/- 11	0.1
1914+149B ^a	49.1903	1.3667	19 14 27.0	14 58 22	0.214	5.1	528 +/- 6	1.9
1914+154	49.5335	1.6473	19 14 05.5	15 24 27	0.690	2.7	158 +/- 7	21.1
1914+158A ^a	50.0147	1.7764	19 14 33.4	15 53 34	0.036	12.6	392 +/- 23	0.3
1914+158B ^a	50.0063	1.7720	19 14 33.4	15 53 00	0.101	13.1	406 +/- 7	1.5
1919+162A ^a	50.9553	0.8511	19 19 48.1	16 17 04	0.041	3.5	515 ^b +/- 51	0.4
1919+162B ^a	50.9535	0.8474	19 19 48.7	16 16 52	0.170	5.9	453 +/- 7	0.6
1922+138A	49.2164	-0.9641	19 22 58.6	13 53 25	0.510	3.6	406 +/- 5	31.2
1922+138B	49.2155	-0.9706	19 22 59.9	13 53 11	0.312	4.2	3 +/- 4	49.2
1929+186A ^a	54.1774	-0.0092	19 29 27.5	18 41 51	0.102	2.0	943 +/- 53	0.6
1929+186B ^a	54.1742	-0.0091	19 29 27.1	18 41 41	0.143	2.6	764 +/- 17	0.7
1938+22A ^a	58.9712	0.2201	19 38 42.0	22 59 04	0.311	4.8	55 +/- 10	1.0
1938+22B ^a	58.9705	0.2179	19 38 42.4	22 58 58	0.058	13.5	75 +/- 21	0.2
1938+22C ^a	58.9757	0.2001	19 38 47.1	22 58 42	0.141	4.8	52 +/- 18	0.6
1939+10A ^a	48.0642	-6.2355	19 39 33.6	10 19 44	0.252	2.1	-201 +/- 13	1.4
1939+10B	48.0624	-6.2346	19 39 33.2	10 19 40	0.339	3.2	204 +/- 14	4.7
1944+25 ^a	62.0833	0.6091	19 44 05.4	25 52 16	0.265	1.1	-127 +/- 23	1.2
1945+24A ^a	60.8084	-0.6335	19 45 57.4	24 08 30	0.042	11.0	-143 ^b +/- 18	1.4
1945+24B ^a	60.7848	-0.6373	19 45 55.1	24 07 10	0.351	1.2	-195 +/- 19	0.1
1945+28 ^a	64.4579	1.5358	19 45 55.1	28 23 14	0.063	6.5	-628 +/- 21	0.3
1948+12 ^a	51.3585	-6.8344	19 48 19.2	12 52 22	0.530	1.0	-54 +/- 13	2.4
1950+25A ^a	62.3759	-0.9548	19 50 42.8	25 19 20	0.138	3.0	-61 +/- 30	0.1
1950+25B ^a	62.3708	-0.9561	19 50 42.4	25 19 02	0.368	6.0	-107 +/- 4	3.6
1950+25C	62.3642	-0.9570	19 50 41.7	25 18 40	0.121	12.4	-87 +/- 5	5.5
1951+27A ^a	64.5704	0.1130	19 51 42.8	27 45 09	0.137	5.2	-150 +/- 7	0.8
1951+27B ^a	64.5719	0.1074	19 51 44.3	27 45 03	0.162	7.4	-149 +/- 5	1.6
1953+28A ^a	65.3277	0.2329	19 53 02.1	28 27 42	0.090	9.6	-65 +/- 8	1.3
1953+28B ^a	65.3258	0.2327	19 53 01.9	28 27 36	0.091	3.5	-91 ^b +/- 67	0.5
1958+30 ^a	67.1748	0.1274	19 57 53.8	29 58 40	0.174	1.4	-41 +/- 16	1.4
2002+335 ^a	70.6772	1.1928	20 02 27.6	33 30 28	0.090	3.0	-47 +/- 60	0.1
2005+403 ^a	76.8239	4.2961	20 05 59.6	40 21 02	3.719	2.2	-137 +/- 4	0.5
2012+234A	63.4042	-6.1191	20 12 17.7	23 25 50	5.160	1.0	-37 +/- 4	28.4
2012+234B	63.4024	-6.1235	20 12 18.4	23 25 36	4.440	0.7	-43 +/- 4	28.9
2013+370 ^a	74.8706	1.2239	20 13 37.0	37 01 44	1.122	0.6	-518 +/- 6	0.7
2015+336A ^a	72.2306	-0.9777	20 15 15.8	33 36 28	1.354	11.7	-390 +/- 4	1.6
2015+336B ^a	72.2311	-0.9824	20 15 17.0	33 36 20	0.585	11.8	-389 +/- 4	3.0
2016+325A ^a	71.5514	-1.8198	20 16 44.8	32 34 18	0.101	10.6	-236 +/- 6	0.1

TABLE 1—Continued

Source	l (deg)	b (deg)	α (1950)	δ (1950)	F (Jy)	P (%)	RM (rad m ⁻²)	χ^2
2016+325B ^a	71.5500	-1.8216	20 16 45.0	32 34 10	0.116	3.2	-283 +/- 19	0.3
2018+296A	69.2179	-3.7623	20 18 02.7	29 33 01	0.389	18.2	-174 +/- 4	9.7
2018+296B	69.2170	-3.7687	20 18 04.0	29 32 45	2.872	0.4	9 +/- 4	127.3
2018+296C	69.2158	-3.7700	20 18 04.1	29 32 39	3.037	3.2	552 +/- 4	36.2
2020+390A ^a	77.3424	1.2495	20 20 38.3	39 04 40	0.093	22.0	-396 +/- 4	0.2
2020+390B ^a	77.3391	1.2532	20 20 36.8	39 04 38	0.070	4.3	-355 +/- 18	0.7
2020+390C ^a	77.3366	1.2538	20 20 36.2	39 04 32	0.050	10.0	-295 +/- 15	0.1
2024+15A	58.2935	-12.9462	20 24 36.0	15 27 23	0.446	1.8	245 +/- 13	11.2
2024+15B ^a	58.2882	-12.9535	20 24 36.8	15 26 53	0.385	1.5	-167 +/- 11	2.3
2024+17 ^a	60.1095	-11.8394	20 24 52.9	17 32 46	0.079	4.3	-151 +/- 8	0.3
2029+20A ^a	63.0199	-11.1679	20 29 22.2	20 16 38	0.069	5.8	-127 ^b +/- 17	2.7
2029+20B ^a	63.0184	-11.1784	20 29 24.2	20 16 12	0.089	4.4	-130 +/- 23	2.4
2034+42A	81.3178	0.9792	20 34 08.9	42 07 40	0.413	1.7	298 +/- 9	22.6
2034+42B	81.3133	0.9649	20 34 11.7	42 06 56	0.302	3.1	-241 +/- 4	116.3
2040+43 ^a	83.1062	0.8053	20 40 52.2	43 26 04	0.043	2.2	-220 +/- 48	0.7
2043+43A ^a	83.4500	0.5016	20 43 21.6	43 30 50	0.152	3.0	-604 +/- 19	0.4
2043+43B ^a	83.4468	0.5029	20 43 20.6	43 30 44	0.257	3.2	-694 +/- 7	2.1
2047+43	83.4099	-0.2761	20 46 32.3	42 59 34	0.924	0.8	180 +/- 11	10.6
2052+46A ^a	86.9909	1.3417	20 52 28.5	46 46 45	0.081	1.5	-588 +/- 38	0.7
2052+46B ^a	86.9855	1.3438	20 52 26.7	46 46 35	0.076	5.0	-646 ^b +/- 28	2.3
2052+46C ^a	86.9795	1.3466	20 52 24.6	46 46 25	0.039	7.3	-639 +/- 32	0.4
2054+47A ^a	87.6463	1.4025	20 54 42.2	47 19 00	0.167	3.6	-881 +/- 11	0.5
2054+47B ^a	87.6438	1.4003	20 54 42.2	47 18 48	0.139	5.8	-862 +/- 8	0.6
2057+48A ^a	88.5908	1.6318	20 57 21.3	48 10 48	0.048	3.8	-689 +/- 37	0.2
2057+48B ^a	88.5895	1.6274	20 57 22.2	48 10 34	0.053	8.8	-716 +/- 22	0.3
2114+49 ^a	91.5547	0.5071	21 14 37.4	49 35 30	0.331	6.8	410 +/- 4	2.8
2117+494A ^a	91.7129	0.0816	21 17 10.4	49 24 19	1.665	10.8	325 +/- 4	2.2
2117+494B ^a	91.7077	0.0860	21 17 07.9	49 24 17	0.683	11.8	385 +/- 4	0.3
2120+49A ^a	91.9576	-0.5294	21 20 52.6	49 08 38	0.135	6.2	345 +/- 10	0.2
2120+49B ^a	91.9557	-0.5299	21 20 52.2	49 08 32	0.486	3.3	318 +/- 4	0.4
2130+32	81.6218	-13.7331	21 30 31.7	32 32 14	0.310	2.2	-101 +/- 9	11.9

^a Selected in final sample of sources.^b Acceptable alternative to minimum χ^2 fit.

also excluded from the large-scale fit. These sources are discussed in § 7.

6. THE LARGE-SCALE FIELD

6.1. Extent of the Field

In Figure 8 we compare the RMs expected from the SF, SK, and RK models with the data. It is immediately evident that none of the models correctly predict the magnitude of RMs observed for longitudes $\gtrsim l_0$. The discrepancy is especially large near $l = 90^\circ$, where the line of sight passes only through the outer galaxy (Galactocentric radii greater than R_0). The magnitude of RM in this direction depends on (1) the average electron density along the line of sight; (2) the average magnetic field strength along the line of sight; (3) the geometry of the field lines; and (4) the maximum extent of the Galactic field.

The true field geometry is unknown. Roughly equal evidence from the field models points to circular and spiral configurations. We adopt a circular field geometry and derive the Galactocentric extent R_m of the magnetoionic medium required to produce the observed RMs. We assume that the average electron density and field strength are equal to the local values of 0.03 cm^{-3} , $2.1 \mu\text{G}$. In fact, n_e and B are likely to decrease at large Galactocentric radii, but in order to derive a lower limit to the field extent we will adopt the local values.

For a line of sight toward 90° longitude, the RM caused by a circular field will be

$$\text{RM}(90^\circ) = -810 \langle n_e \rangle \langle B \rangle R_0 \times \ln [R_m/R_0 + \sqrt{(R_m/R_0)^2 - 1}] \quad (6)$$

where the result is a function of the electron density and the

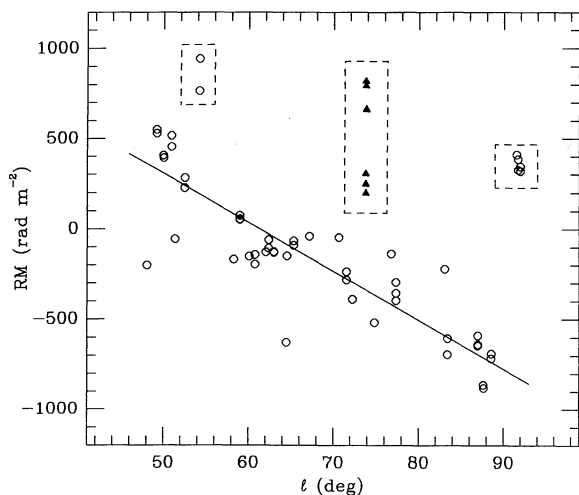


FIG. 5.—Rotation measures vs. Galactic longitude. Open circles are from this work; solid triangles are rotation measures through the Cygnus region from the work of Lazio, Spangler, & Cordes (1990). The line is a least-squares fit to the data (see text), excluding the data points encircled by dashed lines. The excluded sources near $l = 54^\circ$ are extremely low latitude ($b \approx 10^{-2}$), and those near $l = 92^\circ$ are anomalous RMs discussed in § 7. Rotation measure uncertainties (see Table 1) are generally smaller than the data points. The RM of source 1713–342B (-169 rad m^{-2}) at $l = 352^\circ$ is not plotted here.

total magnetic field strength (not the line of sight component) averaged over the line of sight. Using a value $R_m = 15 \text{ kpc}$, which is assumed in most all of the field models proposed to date, yields $\text{RM}(90^\circ) = -490 \text{ rad m}^{-2}$. Note that this is a conservative upper limit to the magnitude of RM in this direction, since, as mentioned above, we have used the local values of $\langle n_e \rangle$ and $\langle B \rangle$ which are almost certainly too large for a line of sight through the outer Galaxy. From equation (5), we see that the observed RM toward $l = 90^\circ$ is $\text{RM}(90^\circ) = 1607(1.08 - \pi/2) \approx -788 \text{ rad m}^{-2}$. Reconciliation with equation (6) requires $R_m/R_0 = 2.5$, or $R_m = 25 \text{ kpc}$. This is a lower limit to R_m under the assumption of a circular field geometry because of the values of $\langle n_e \rangle$ and $\langle B \rangle$ we have assumed. (Note

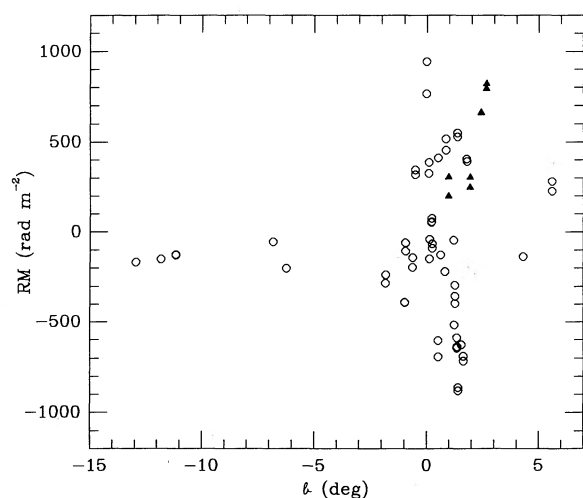


FIG. 6.—Rotation measures vs. Galactic latitude. Open circles are from this work; solid triangles are from Lazio, Spangler, and Cordes (1990) and arise from the Cygnus region (see text). Error bars on the individual RMs are generally smaller than the data points; Table 1 lists the computed uncertainties.

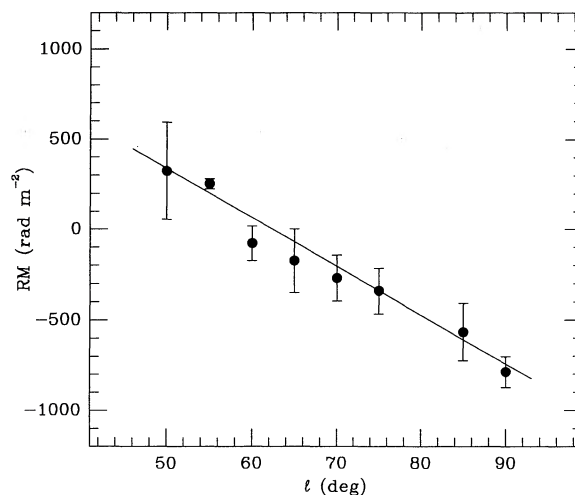


FIG. 7.—Rotation measure as a function of Galactic longitude, obtained by averaging the data of Fig. 5 in bins of width 5° (no sources lie within 2.5° of $l = 80^\circ$). The error bars are ± 1 standard deviation for the data in each bin. Data enclosed by dashed lines in Fig. 5 were excluded. A least-squares fit to the unbinned rotation measures is indicated.

that even if we make the unreasonable assumptions that the field is perfectly aligned along the $l = 90^\circ$ line of sight, with no curvature to the field lines out to the edge of the Galaxy, and that n_e and B remain constant over the line of sight, we still derive $R_m = 18 \text{ kpc}$.

This field extent is much farther than that determined from or assumed in other models of the Galactic magnetic field. We argue that previous RM surveys have been insensitive to Galactic fields beyond $\sim 15 \text{ kpc}$. Extragalactic RMs obtained previous to this survey were concentrated at $|b| > 10^\circ$. Given a scale height for the magnetoionic medium of $\approx 1 \text{ kpc}$ (SK, IT, SF), the lines of sight toward the sources sample the field out to a distance projected on the Galactic plane of $\approx 5.7 \text{ kpc}$ before extending beyond the magnetoionic layer. The data therefore probe the field out to a maximum distance (toward the Galactic anticenter) of $R_0 + 5.7 = 15.7 \text{ kpc}$, and closer in for other directions ($R_0 - 5.7 = 4.3 \text{ kpc}$ toward the Galactic center).

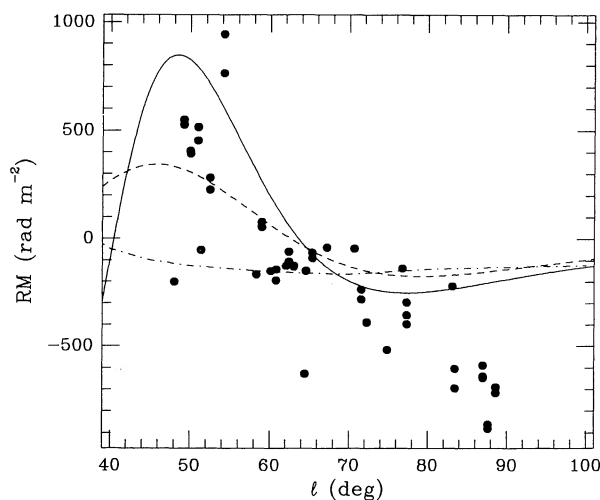


FIG. 8.—Comparison of observed RMs with those expected from the models of SF (solid line), RK (dashed line), and SK (alternating dash-dot line). The anomalous RMs at $l = 92^\circ$ are not plotted.

Pulsar data are obtained at $|b| \lesssim 10^\circ$, but relatively few pulsars are known at $R > 15$ kpc, so models derived from pulsar data are also insensitive to the field at large R .

The large extent of the magnetoionic disk is very surprising especially because it is now believed that most of the warm ionized interstellar medium is due to ionization by hot stars, the number density of which has a strong radial dependence. Thus the large value of R_m indicates that both ionized gas and magnetic fields exist in the outer regions. The implications of this conclusion will be addressed in a future paper (Clegg et al. 1991).

6.2. Field Reversals and the NPS

A null in $RM(l)$ clearly exists at $l = l_0 = 62^\circ$. The null likely results from equal and opposite RM contributions from reversed field regions along the line of sight. Such reversals have been established on the basis of pulsar data (RK) where distance information is available. The longitude of the null is an important observable because of its dependence on the distance to the field reversal, the relative amplitudes of the inner and outer fields B_i and B_o , and the inner and outer electron densities n_i and n_o , and the total extent of the field along the line of sight. We investigate the existence of this null in terms of the concentric ring field model with a reversal in field direction interior to R_0 . Using $R_m = 25$ kpc as derived above, we find that the null cannot exist at 62° in a model where the product $n_e B$ interior and exterior to the field reversal has equal magnitude with opposite sign. The average magnitude in the interior (reversed) region must be *greater* than that outside the reversal in order for a null to be produced. (Note that this result takes into account the $B \cdot dl$ geometrical effect).

The analysis of SF suggests that the average field strength and electron density decrease with Galactocentric radius R as $1/R$. If we incorporate this scaling in a circular field model, and further assume (from RK) that the azimuthal field varies sinusoidally with R with wavelength $\Delta = 6200$ pc {i.e., $n_e B \propto (1/R^2) \cos [2\pi(R - R_r)/\Delta]$, with R_r the radius at which the reversal occurs}, we find that the null at 62° requires a field reversal at distance $d_r = 660$ pc measured toward the Galactic center, corresponding to a Galactocentric radius $R_r = 9340$ pc. Our result is consistent with RK's analysis in which $d_r = 650 \pm 90$ pc. SF's spiral model requires $d_r = 1.2$ kpc. SK's large value of $d_r \simeq 2$ kpc is the reason that they expect negative RMs throughout the region studied here (see Fig. 8), when in fact large positive RMs are observed for $l < l_0$. In their model, the line of sight passes into the reversed field only for $l \lesssim 40^\circ$. We believe that the distance they derive to the field reversal is overestimated. Using RK's model strictly (sinusoidal variation of $n_e B$ with no $1/R$ dependence), the reversal must lie at a distance $d_r = 565$ pc, which is also consistent within errors with their result. In either case, either by the $1/R$ scaling plus sinusoidal variation in B or by the sinusoidal variation alone, the magnitude of $n_e B$ through the field-reversed region must on average be greater than that at R_0 .

An additional contribution to the positive RMs in the first quadrant may arise from the NPS. This conclusion has been drawn in the derivation of field models by noting the lack of symmetry of $RM(l)$ in the north Galactic hemisphere in comparison to $RM(l)$ observed in the southern hemisphere, and the correspondence of the deviation with the position of the NPS as ascertained from radio continuum data. The effect of the NPS on RMs at low latitudes (i.e., within 10° of the plane) has not been firmly established due to the lack of a large number of

data points. The NPS contribution at high latitudes has been estimated at ~ 5 rad m^{-2} with an internal field strength of $6 \mu G$ (Vallée 1984), which would lead us to believe its effect on our data is small, considering the much larger ~ 160 rad m^{-2} spread in RM about our large-scale fit due to small-scale variations in the field. We note, however, a bias in the *residuals* to our large-scale fit which suggests a net positive offset in RMs in the northern hemisphere. Specifically, we find that at $b < 0^\circ$, 13 of 16 sources possess negative residuals about the large-scale fit, which is a 2.5σ increase in the number of negative residuals expected (50%) from a random distribution. In comparison, 14 out of 34 sources in the northern hemisphere have negative residuals (0.7σ fewer than the number expected). We have excluded the anomalous RMs near $l = 92^\circ$. At this point, we are unable to ascertain if the bias is due to the NPS.

6.3. Comparison with Pulsar Data Along Specific Lines of Sight

We have compared pulsar and extragalactic RMs along nearly identical lines of sight (to within 3°) near $l \simeq 70^\circ$ and 87.5° (Fig. 9). The lines of sight are dictated by the coincidence of our extragalactic RMs with existing pulsar data. While few data points exist, we make a preliminary inference based on the available data. Along both lines of sight, the magnitudes and signs of extragalactic RMs are inconsistent with the values expected from the trend of the pulsar data. At 87.5° longitude in particular, the pulsar RMs increase weakly with distance while the extragalactic RMs are large and negative. The difference between the 5 kpc pulsar and the extragalactic sources is substantial (nearly 10^3 rad m^{-2}) and suggests that there may be a reversal in the field orientation in this direction beyond a line-of-sight distance of 5 kpc, or a Galactocentric radius of $\gtrsim 11$ kpc. The possibility of a reversal exterior to the solar circle was noted by RK, and the present data reinforce the argument for its existence.

A similar comparison is made for two lines of sight at 50° and 54.2° longitude (Fig. 10). The dependence on distance of pulsar RMs along these lines of sight is more complicated due to the interior field reversal but we note that extragalactic RMs are consistent with the general trends of pulsar RMs at dis-

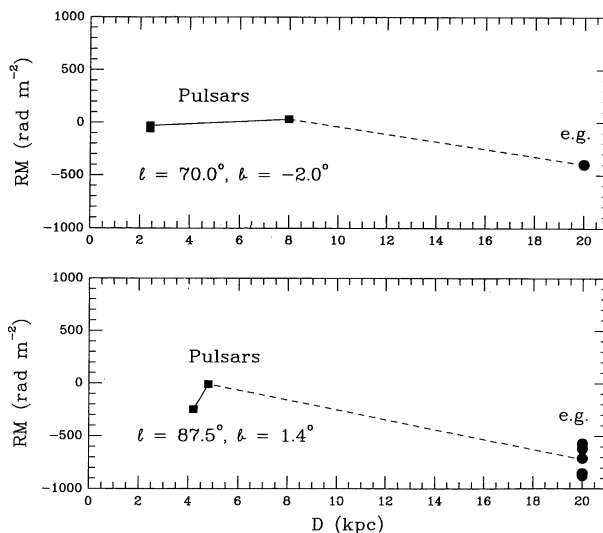


FIG. 9.—Comparison of extragalactic and pulsar RMs along lines of sight within 3° of $(l, b) = (70^\circ, -2^\circ)$ (top) and $(87.5^\circ, 1.4^\circ)$ (bottom). The extragalactic sources are plotted at an arbitrary distance of 20 kpc.

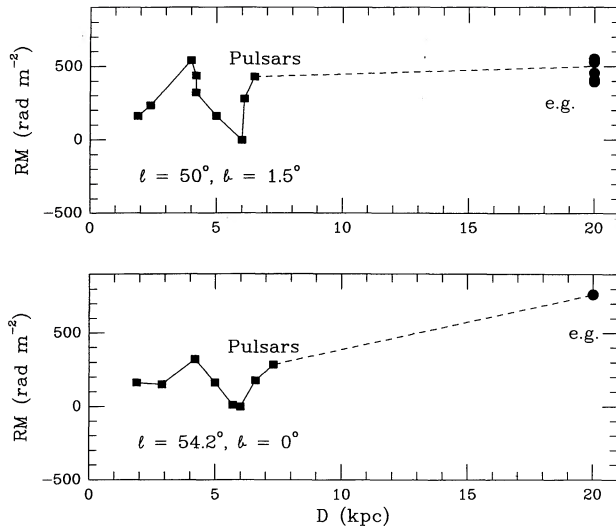


FIG. 10.—Comparison of extragalactic and pulsar RMs along lines of sight within 3° of $(l, b) = (50^\circ, 1.5^\circ)$ (top) and $(54.2^\circ, 0^\circ)$ (bottom). The extragalactic sources are plotted at an arbitrary distance of 20 kpc.

tance ≥ 8 kpc. There is no indication that field reversals occur at large Galactocentric radius in this direction. However, it is much harder to locate an exterior field reversal at $l = 50^\circ$, where a larger contribution to RM arises from the inner Galaxy, than at $l = 70^\circ$, which mostly probes the outer Galaxy.

7. ANOMALOUS ROTATION NEAR $l = 92^\circ, b = 0^\circ$

An anomalous RM contribution of magnitude $\sim +1000$ rad m^{-2} is noted near $l = 92^\circ, b = 0^\circ$. Five sources in this region exhibit large positive RMs of nearly similar amplitude. The rotation is opposite in sign to the prevailing field in this region and is evidence for a localized field reversal with a large value of $n_e B_{\parallel}$. To our knowledge, this anomaly has not been reported previously. One of the sources, 2117+49, was observed in the survey of Simard-Normandin et al. (1981), but was subsequently discarded in SK's selection process because of its difference with surrounding RMs. Simard-Normandin et al. (1981) list a RM for this source of 347 rad m^{-2} , while we have resolved it into two components with RMs of 325 and 385 rad m^{-2} .

The mean position of this group of anomalous sources is $l = 91^\circ.78, b = -0^\circ.8$, with spread in l and b of $0^\circ.4$ and 1° , respectively. Other sources located approximately 8° from the affected group exhibit rotation measures consistent with expected values based on the general trend of RM with longitude (Fig. 5).

The magnitude of $n_e B_{\parallel}$ for this anomaly can be crudely estimated if its scale sizes perpendicular and parallel to the line of sight are assumed equal. Then $n_e B_{\parallel} = 1.23 \Delta\text{RM}/\theta D$, where ΔRM is the excess rotation measure and θ is the angular extent of the region at a distance D in parsecs. We have $\Delta\text{RM} \approx 1000 \text{ rad m}^{-2}$ and $1^\circ \lesssim \theta \lesssim 8^\circ$. The distance is unknown but if the region is presumed to be associated with the intersection of our line of sight with the nearby Perseus spiral arm, then $D \approx 3$ kpc. In this case, $3 \text{ cm}^{-3} \mu\text{G} \lesssim n_e B_{\parallel} \lesssim 24 \text{ cm}^{-3} \mu\text{G}$.

A localized magnetohydrodynamic disturbance is likely to affect n_e and B simultaneously, so that it is difficult to decouple the magnitude of the electron density fluctuation from magnetic field enhancement. We can compare thermal electron pressure to magnetic energy density and the self-gravitational

“pressure” of the anomaly to derive approximate equilibrium values of n_e and B . The ratio of thermal electron pressure at 10^4 K to magnetic energy density is

$$\frac{P_T}{P_B} \approx 5 \left(\frac{n_e}{\text{cm}^{-3}} \right) \left(\frac{B_{\parallel}}{\mu\text{G}} \right)^{-2}, \quad (7)$$

while the ratio of gravitational to thermal pressure is

$$\frac{P_g}{P_T} \approx 6.7 \times 10^{-6} \left(\frac{\Delta\text{RM}}{\text{rad m}^{-2}} \right) \left(\frac{R}{\text{pc}} \right) \left(\frac{B_{\parallel}}{\mu\text{G}} \right)^{-1}. \quad (8)$$

In the observed anomaly, equipartition between thermal and magnetic pressures is achieved for $n_e \approx 1\text{--}5 \text{ cm}^{-3}$, $B_{\parallel} \approx 2.5\text{--}5 \mu\text{G}$. If n_e is substantially larger, thermal expansion can disrupt the feature on short time scales, while ambient magnetic fields greater than $\sim 5 \mu\text{G}$ increase its longevity. The gravitational pressure is $\approx 0.1\text{--}1 P_T$ for $B_{\parallel} = 3 \mu\text{G}$ and $R = 50\text{--}400$ pc. Spitzer (1978) demonstrates that diffusion time scales for interstellar clouds are generally longer than time scales for dynamical processes, at least in the limit of ideal cloud geometries. Without additional information, it is difficult to determine the importance of diffusion in the stability of the observed anomaly.

Infrared observations of the region at $25\text{--}100 \mu\text{m}$ obtained with *IRAS* show a nearby dust complex that is probably associated with a star-forming region. However, many of our sources viewed through the Galactic plane exhibit a similar juxtaposition. There are no associated features on the Palomar Sky Survey plates, no localized enhancement in $\text{H}\alpha$ emission is noted in the survey of Reynolds (1983) and no obvious enhancement in the 408 MHz synchrotron continuum (Phillips et al. 1981).

Lazio, Spangler, & Cordes (1990) have determined rotation measures of extragalactic sources viewed near or behind the Cygnus region. Their data are plotted in Figures 5 and 6. The Cygnus region is responsible for greatly enhanced scattering measures of background objects. In analogy with the anomalous RMs reported here, the Cygnus complex adds a large positive component to Faraday rotation compared to other sources viewed along similar lines of sight. The rotation is particularly enhanced for two of their sources located just outside the boundary of intense optical emission delineated by Palomar survey prints. The results are direct evidence that enhanced RMs are associated with enhancements in n_e and B at the periphery of regions replete with OB associations, stellar winds, and expanding SNRs.

The observed ΔRM for the Lazio et al. (1990) sources is similar to that observed for the region reported here. Not immediately evident in IR or optical images, our anomalous region is most likely more distant than the Cygnus complex. Given its greater angular size, the value of $n_e B_{\parallel}$ for Cygnus is comparable to that derived for the region reported here. The origin of anomalous RMs is conceivably a more distant complex akin to the Cygnus region.

8. SMALL-SCALE VARIATIONS

The variations in rotation measure over an angular scale $\delta\theta$ are quantified through the *structure function*, $D(\delta\theta)$, where

$$D(\delta\theta) \equiv \langle [RM(\theta) - RM(\theta + \delta\theta)]^2 \rangle. \quad (9)$$

The structure function is estimated by computing angular separation $\delta\theta$ and squared differences in rotation measure

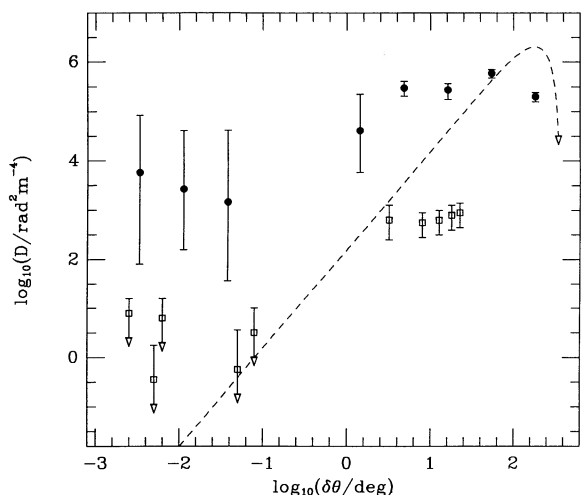


FIG. 11.—Structure function (eq. [9]) of the rotation measure data (solid circles). The error bars are ± 1 standard deviation for $\delta\theta > 1^\circ$ and show the total range of observed ΔRM^2 for $\delta\theta < 1^\circ$, where each structure function bin is comprised of relatively few data points. The anomalous RMs at $l = 92^\circ$ were not used in the computation of the structure function. For comparison, the structure function of RMs for sources at high Galactic latitudes (Simonetti & Cordes 1986) is shown (hollow squares) with 1σ error bars. The geometric contribution to the low-latitude structure function from a perfectly uniform large-scale field (D_g , eq. [10]) is indicated (dashed line).

ΔRM^2 between all pairs of sources. The data $\Delta\text{RM}^2(\delta\theta)$ are binned in $\delta\theta$ into logarithmic bins of width $\Delta \log(\delta\theta/\text{deg}) \approx 0.5$. Within each bin, the structure function is computed from $D(\delta\theta) \equiv \langle \Delta\text{RM}^2(\delta\theta) \rangle$. The structure function of our data is plotted in Figure 11. Sources with $|b| > 5^\circ$ and the anomalous sources near $l \approx 92^\circ$, $b \approx 0^\circ$ were not used in the computation. We have also plotted the structure function of high-latitude sources from Simonetti & Cordes (1986).

At large angular separations ($\delta\theta \gtrsim 1^\circ$), the structure function due to a perfectly uniform field will have a substantial geometrical component due simply to the change in $\mathbf{B} \cdot d\mathbf{l}$. An observer embedded in an extended homogeneous medium with uniform magnetic field approaching from an arbitrary angle θ_0 sees a rotation measure $\text{RM}_0 \cos(\theta - \theta_0)$, where RM_0 is the rotation measure toward θ_0 . The structure function is computed by averaging rotation measure differences across angular scales $\delta\theta$ over $0 \leq \theta \leq 2\pi$. In this first-order approximation of a large-scale Galactic field, the geometric contribution to the structure function is

$$D_g(\delta\theta) \equiv \text{RM}_0^2(1 - \cos \delta\theta). \quad (10)$$

For $\delta\theta \ll 90^\circ$, $D(\delta\theta) = \text{RM}_0^2 \delta\theta^2/2$. The result is modified if the field is not sampled over all θ . If the line of sight is predominantly perpendicular to the field lines, then $\text{RM} \approx \text{RM}_0 \delta\theta$, and $D(\delta\theta) = \text{RM}_0^2 \delta\theta^2$, which is a factor of 2 greater than equation (10) for small $\delta\theta$. If the line of sight is roughly parallel to the field lines, then $\text{RM} \approx \text{RM}_0 \cos(\delta\theta)$, and $D(\delta\theta) = \text{RM}_0^2 \delta\theta^4/4$ at small $\delta\theta$, which is \ll equation (10). Our sample is somewhere between the two extremes, since the local field points along $l \approx 90^\circ$ and the distant field becomes closer to perpendicular to the line of sight. We take equation (10) as a conservative upper limit to the true structure function.

In Figure 11, the dashed line is a comparison of equation (10) with the computed structure function of our data, using $\text{RM}_0 = 10^3 \text{ rad m}^{-2}$ obtained from canonical values of electron density, magnetic field strength, and path length (0.03 cm^{-3} , $2.1 \mu\text{G}$, 20 kpc).

8.1. Structure on Angular Scales $\delta\theta > 1^\circ$

For $\delta\theta > 1^\circ$, the structure functions of low- and high-latitude RMs differ by an average factor of $\gtrsim 10^3$. We show that a significant part of the difference arises from the random contribution to RMs from structure in $n_e B_{\parallel}$ on small angular scales.

The structure function can be expressed as the sum of three contributions:

$$D(\delta\theta) = D_g(\delta\theta) + D_s(\delta\theta) + D_i, \quad (11)$$

where D_g , the geometrical term, is approximated by equation (10), D_s is a statistical term due to fluctuations in RM on scales $\lesssim \delta\theta$, and D_i is the contribution to the structure function from intrinsic RMs. If the intrinsic RM is denoted by RM_i , then $D_i = 2\langle \text{RM}_i^2 \rangle$; similarly $D_s = 2\langle \text{RM}_s^2 \rangle$ where RM_s is the statistical contribution to RM from fluctuations on angular scales smaller than the typical separation between sources. SK notes that the amplitude of RM_i is $\lesssim 10 \text{ rad m}^{-2}$ so that $D_i \lesssim 200 \text{ rad}^2 \text{ m}^{-4}$. Over angular scales considerably less than 90° , the geometrical contribution to the structure function at high latitudes is very small since $\text{RM}_0 \lesssim 30 \text{ rad m}^{-2}$ (Simonetti & Cordes 1986). For example, at $\delta\theta = 10^\circ$, $D_g \approx 14 \text{ rad}^2 \text{ m}^{-4}$. This is a small fraction of the observed structure function of $10^3 \text{ rad}^2 \text{ m}^{-4}$.

From these estimates of the geometrical and intrinsic contributions to D we can estimate the statistical contribution at high latitudes. We find $D_s = D - D_g - D_i \approx 1000 - 14 - 200 = 786 \text{ rad}^2 \text{ m}^{-4}$, which gives $\text{RM}_s \equiv (D_s/2)^{1/2} \approx 20 \text{ rad m}^{-2}$. Since this is considerably less than the 160 rad m^{-2} fluctuation in RM about our large-scale fit at low latitudes, we conclude that RMs are not only larger at low latitudes, but that the fluctuations in RM are larger as well. The discrete structures such as supernova remnants and stellar winds that are responsible for the RM fluctuations are more prevalent at lower latitudes, which is one explanation of our result.

8.2. Structure on Angular Scales $\delta\theta < 1^\circ$

We investigate small-scale field structure by examining differences in rotation measures between lobes of multi-component extragalactic sources. The angular separations range from 10^{-3} to 0.1 , and probe transverse physical length scales as small as 0.1 – 10 pc at 5 kpc . Observed differences are as large as 180 rad m^{-2} and are significantly greater than intrinsic RMs of extragalactic sources ($\lesssim 10 \text{ rad m}^{-2}$). Expected ΔRMs across lobes due to geometrical effects are exceedingly small (0.02 rad m^{-2} for $\delta\theta = 40^\circ$). The divergence between the geometric structure function (eq. [10]) and the observed structure function for angles $\ll 1^\circ$ is clearly evident in Figure 11. The difference is more than about four orders of magnitude, and implies that at small angular separations, rotation measure differences are completely dominated by deviations from a uniform field/homogeneous medium.

We believe that the differences in RM between lobes of the extragalactic sources are induced by interstellar fluctuations in $n_e B_{\parallel}$ rather than intrinsic variations in RM. There are at least two arguments supporting this assumption: (1) intrinsic RMs are typically less than 10 rad m^{-2} (SK) which is less than most of the observed differences in RM (2) differences in RM on small angular scales are greater at low latitudes than those measured at high latitudes by Simonetti & Cordes (1986). This would not be expected if the predominant contribution to the differences was intrinsic to the sources.

The small-scale variations in the magnetoionic medium are likely related to electron density fluctuations in the ISM which

have been studied through scattering and scintillation observations (Rickett 1990). The density fluctuations are usually postulated to follow a power-law spectrum in wavenumber q (\sim inverse length scale) over a range (q_0, q_1),

$$P_{\delta n_e} = C_N^2 q^{-\alpha}, \quad (12)$$

with the exponent $\alpha \simeq 11/3$ (Kolmogorov turbulence). The position-dependent normalization factor C_N^2 determines the total power in the fluctuations and is derivable from pulsar scattering and scintillation measurements. Simonetti, Cordes, & Spangler (1984) and Leahy (1987) have shown that the structure function of rotation measures in specific regions of the sky is approximately consistent with a power-law spectrum of turbulence in the quantity ($n_e B_{\parallel}$).

We use this form of the spectrum with observational constraints on C_N^2 , q_0 , and q_1 to approximate the contribution to small-scale RM variations solely from electron density turbulence. With a power-law distribution of irregularities the exact form of the statistical contribution to the rotation measure structure function (Simonetti & Cordes 1988) is

$$D_s(\delta\theta) = 2.88 \times 10^5 \left(\frac{C_N^2}{\text{m}^{-20/3}} \right) \left(\frac{\langle B_{\parallel} \rangle}{\mu\text{G}} \right)^2 \left(\frac{\delta\theta}{\text{deg}} \right)^{5/3} \left(\frac{L}{\text{kpc}} \right)^{8/3} \text{rad}^2 \text{m}^{-4}, \quad (13)$$

where L is the line-of-sight path length. The structure function $D(\delta\theta) \simeq \sigma_{\text{RM}}^2(\delta\theta)$, where $\sigma_{\text{RM}}^2(\delta\theta)$ is the variance in RM over angular scales $\lesssim \delta\theta$. Fluctuations due to electron density turbulence occur over angular scales $l_1/L \ll \delta\theta \ll l_0/L$, where $l_0 = 2\pi/q_0$, $l_1 = 2\pi/q_1$ are respectively the outer and inner scale sizes for the fluctuations. The scattering data indicate that $l_1 \ll l_0$, so σ_{RM} produced solely by electron density turbulence for projected separations much greater than the outer scale is approximately

$$\sigma_{\text{RM}} \simeq 35 \text{ rad m}^{-2} \left(\frac{\text{SM}}{\text{m}^{-20/3} \text{ kpc}} \right)^{1/2} \left(\frac{\langle B_{\parallel} \rangle}{\mu\text{G}} \right) \left(\frac{l_0}{\text{pc}} \right)^{5/6}. \quad (14)$$

We have introduced the *scattering measure* $\text{SM} \equiv \int C_N^2 dl$ evaluated along the line of sight, which is given by angular broadening and scintillation observations of background sources. Cordes et al. (1991) list SMs for several of the extragalactic sources observed in this survey. For example, 1849+005, 2005+403, and 1213+370 have $\text{SM} = 380, 0.44$, and $0.15 \text{ m}^{-20/3} \text{ kpc}$, respectively, which predict $\sigma_{\text{RM}} \simeq 1300, 50$, and 27 rad m^{-2} for $B_{\parallel} = 2 \mu\text{G}$ and outer scale length $l_0 = 1 \text{ pc}$. Typical SMs for other low-latitude first quadrant extragalactic sources in the data of Cordes et al. (1991) are $\simeq 1 \text{ m}^{-20/3}$, giving typical $\sigma_{\text{RM}} \simeq 100 \text{ rad m}^{-2}$, although the range in observed SMs is three orders of magnitude. The point is that the computed σ_{RM} 's are, at the least, a sizable portion of the $\simeq 160 \text{ rad m}^{-2}$ residual to the large-scale fit (eq. [5]). We conclude that electron density turbulence, as delineated from interstellar scattering and scintillation phenomena, can alone account for much of the small-scale fluctuations in rotation measure seen in the low-latitude extragalactic sources. (It is difficult to ascertain the effect of magnetic field fluctuations on the observed σ_{RM} . Fluctuations in n_e are almost certainly accompanied by variations in B , but the relation between δn_e and δB is unclear. The scatter in RM will be larger if enhancements in B are linked to enhancements in n_e , and less if one enhancement occurs at the expense of the other).

Cordes, Clegg, & Simonetti (1990) have estimated the relative energy densities invested in small-scale and large-scale

magnetic fields in the Galaxy, assuming a Kolmogorov-type spectrum for fluctuations in the product quantity $\delta(n_e B_{\parallel})$. The rms electron density, δn_e , and rms magnetic field amplitude, δB , can be related by

$$\left(\frac{\delta n_e}{n_e} \right) = \zeta \left(\frac{\delta B}{B} \right)^n, \quad (15)$$

with previous work suggesting $\zeta \simeq 1$, $n = 2$ for MHD turbulence (continuum of fluctuation scales in B), or $n = 1$ for obliquely propagating MHD waves (S. R. Spangler 1989, private communication). With a Kolmogorov spectrum of $n_e B$ fluctuations, the relative energy densities in magnetic field fluctuations ($U_{\delta B}$) and the large-scale field (U_B) is

$$\frac{U_{\delta B}}{U_B} = \left[0.55 \left(\frac{C_N^2}{\text{m}^{-20/3}} \right) \left(\frac{l_0^{2/3}}{\zeta^2 n_e^2} \right) \right]^{1/n}. \quad (16)$$

The ratio is $\simeq 1$ for canonical values of C_N^2 , l_0 , and n_e ($10^{-3.5} \text{ m}^{-20/3}$, 1 pc , 0.025 cm^{-3} , respectively), and $\zeta = 1$. The result suggests that comparable energy is invested in small- and large-scale magnetic field structure in the ISM.

9. CONCLUSIONS

Reliable RMs for 56 components of 33 extragalactic sources have been measured. All except one of the objects are in the range $45^\circ < l < 93^\circ$. Of the 33 sources, most are within 5° of the plane; 13 are single component sources or multicomponent sources for which we obtained a reliable RM for one component, 17 are double component sources, three are triple com-

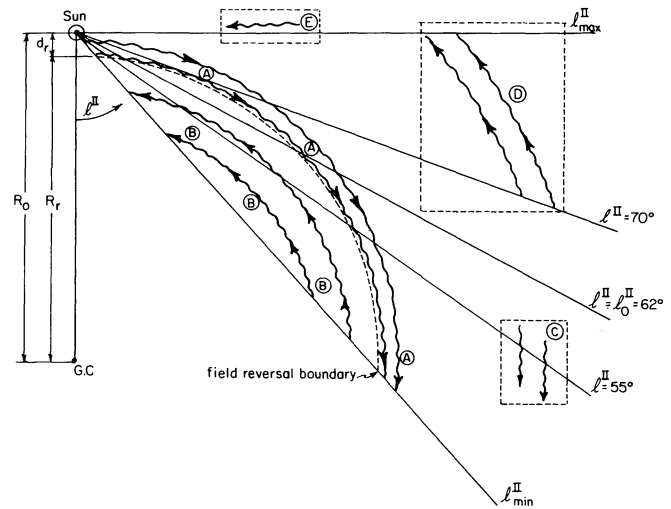


FIG. 12.—Schematic summary of the Galactic field structure ascertained from the data presented here. The conclusions are summarized in the text (§ 9). The position of the Sun is indicated and lies a distance R_0 from the Galactic center. The mean sense of the field is away from the observer (negative RM) for $l > 62.1^\circ$ (A). At a boundary R_r (dashed curve) from the Galactic center, the field reverses (B); see text for value of R_r . The reversed field region produces positive RMs for $l < 62.1^\circ$. From extragalactic and pulsar data, we determine that toward $l \simeq 55^\circ$, the field maintains its average sense for a great distance (C, surrounded by dashed lines to indicate uncertainty in extent and position along line of sight). At some unknown distance for $l > 70^\circ$, the pulsar and extragalactic data indicate that the predominant sense of the field may reverse (D) for distances $\geq 8 \text{ kpc}$. An anomalous large positive RM is observed toward $l = 92^\circ$ (E). Small-scale structure in the Galactic field is characterized by random distortions in the field lines. The large-scale field has been drawn circularly symmetric about the Galactic center for convenience only. Its true geometry is not clear.

ponent sources. Component separations are as small as $\sim 30''$. The data constitute an important complement to existing RM data because there are few published RMs for low-latitude extragalactic sources.

Our main conclusions regarding the Galactic magnetic field are summarized here and are represented schematically in Figure 12. The large-scale field must extend to Galactocentric radius $R_m \geq 25$ kpc to explain the observed magnitudes of the RMs. Our estimate of R_m is a lower bound due to the possible existence of field reversals or a decline in mean electron density and/or magnetic field strength beyond R_0 . Previous RM studies assumed $R_m \approx 15$ kpc, and we have shown that in fact they were *insensitive* to the magnetoionic medium beyond this distance. Over the observed longitude range, the rotation measures are well described by $RM(l) = 1607 \text{ rad m}^{-2} \sin(l_0 - l)$, with an rms spread about this fit of 157 rad m^{-2} . The null at $l_0 = 62^\circ$ is produced by equal and opposite contributions to RM along the line of sight by a region of reversed field direction interior to R_0 . The null cannot exist if the product $n_e B$ is constant with Galactocentric radius, but requires that n_e and/or B is greater within the inner region. If $n_e B \propto 1/R^2$, the field reversal occurs at a distance of 660 pc interior to R_0 . We have compared extragalactic and pulsar RMs along lines of sight that are coincident to within 3° . The comparison suggests that a field reversal occurs outside of R_0 for $l \gtrsim 70^\circ$, while for smaller l , where the reversal is harder to detect, no evidence for its existence is found. An anomalous contribution to RM of

$+1000 \text{ rad m}^{-2}$ is found over a section of sky between 1° and 8° in extent, located at $l = 92^\circ$, $b = 0^\circ 0'$. Equilibrium requires $n_e \approx 1\text{--}5 \text{ cm}^{-3}$, $B_{\parallel} = 2.5\text{--}5 \mu\text{G}$. The region is akin to the nearby Cygnus complex in its effect on RMs, but it is not immediately evident in H α , infrared, or radio continuum maps.

The spread in RM about our large-scale fit confirms that the magnetoionic medium has a substantial random component. Structure function analysis of the RM between lobes of multi-component sources shows that differences between RMs over small angular scales is more than about four orders of magnitude greater than that expected due to a perfectly uniform field. Observed interstellar electron density turbulence can alone account for the random fluctuations in RM. We have shown that if the magnetoionic medium is turbulent with a Kolomogorov spectrum of fluctuations in $n_e B$, then comparable amounts of energy are invested in the large- and small-scale magnetic field.

This research has benefitted from discussions with Carl Heiles, Joe Lazio, and Steve Spangler. We thank Mary Stevens and Carl Heiles for supplying preliminary observations. A. W. C. is supported by a National Research Council/Naval Research Lab cooperative research associateship. J. M. C. acknowledges support from NSF grant AST 85-20530 and NASA grant NAGW-1646. S. R. K.'s work is supported by an NSF Presidential Young Investigator Award and an Alfred P. Sloan Foundation research fellowship.

REFERENCES

- Bevington, P. 1969, *Data Reduction and Error Analysis for the Physical Sciences* (New York: McGraw-Hill)
- Clark, B. G. 1980, *A&A*, 89, 377
- Clegg, A. W. 1991, Ph.D. thesis, Cornell Univ.
- Clegg, A. W., Kulkarni, S. R., & Cordes, J. M. 1991, in preparation
- Cordes, J. M., Clegg, A. W., & Simonetti, J. H. 1990, *IAU Symp. 140, Galactic and Intergalactic Magnetic Fields*, ed. R. Beck, P. P. Kronberg, & R. Wielebinski (Dordrecht: Reidel), 55
- Cordes, J. M., Weisberg, J., Frail, D. A., Spangler, S., & Ryan, M. 1991, *Nature* in press
- Gardner, F. F., & Whiteoak, J. B. 1966, *ARA&A*, 4, 245
- Garwood, R., Dickey, J. M., & Perley, R. 1986, *BAAS*, 18, 690
- Hamilton, P. A., & Lyne, A. G. 1987, *MNRAS*, 224, 1073
- Heiles, C. 1987, in *Interstellar Processes*, ed. D. J. Hollenbach & H. A. Thronson, Jr. (Dordrecht: Reidel), 171
- Inoue, M., & Tabara, H. 1981, *PASJ*, 33, 603 (IT)
- Kronberg, P. P., Conway, R. G., & Gilbert, J. A. 1972, *MNRAS*, 156, 275
- Kulkarni, S. R., & Heiles, C. 1988, in *Galactic and Extragalactic Radio Astronomy*, ed. G. L. Verschuur & K. I. Kellerman (New York: Springer), 95
- Lazio, T. J., Spangler, S., & Cordes, J. M. 1990, *ApJ*, 363, 515
- Leahy, J. P. 1987, *MNRAS*, 226, 433
- Lyne, A. G., & Smith, F. G. 1989, *MNRAS*, 237, 533
- Manchester, R. N. 1974, *ApJ*, 188, 637
- Napier, P. J., & Crane, P. C. 1982, *Synthesis Mapping*, ed. A. R. Thompson & L. R. D'Addario (Green Bank: NRAO), 3-1
- Phillips, S., Kearsy, S., Osborne, J. L., Haslam, C. G. T., & Stoffel, H. 1981, *A&A*, 98, 286
- Rand, R. J., & Kulkarni, S. R. 1989, *ApJ*, 343, 760 (RK)
- Reynolds, R. J. 1983, *ApJ*, 268, 698
- Rickett, B. J. 1990, *ARA&A*, 28, 561
- Simard-Normandin, M., & Kronberg, P. P. 1980, *ApJ*, 242, 74 (SK)
- Simard-Normandin, M., Kronberg, P. P., & Button, S. 1981, *ApJS*, 45, 97
- Simonetti, J. H., & Cordes, J. M. 1986, *ApJ*, 310, 160
- . 1988, *Amer. Inst. Physics Conf. 174, Radio Wave Scattering in the Interstellar Medium*, ed. J. M. Cordes, B. J. Rickett, & D. C. Backer (New York: American Institute of Physics), 134
- Simonetti, J. H., Cordes, J. M., & Spangler, S. R. 1984, *ApJ*, 284, 126
- Sofue, Y., & Fujimoto, M. 1983, *ApJ*, 265, 722 (SF)
- Spitzer, L., Jr. 1978, *Physical Processes in the Interstellar Medium* (New York: John Wiley)
- Tabara, H., & Inoue, M. 1980, *A&AS*, 39, 379
- Thompson, A. R., Moran, J. M., & Swenson, G. W., Jr. 1986, *Interferometry and Synthesis in Radio Astronomy* (New York: John Wiley)
- Thomson, R. C., & Nelson, A. H. 1980, *MNRAS*, 191, 863 (TN)
- Vallée, J. P. 1980, *A&A*, 86, 251
- . 1984, *A&A*, 136, 373
- Zweibel, E. G. 1987, in *Interstellar Processes*, ed. D. J. Hollenbach & H. A. Thronson, Jr. (Dordrecht: Reidel), 1195